ECS Journal of Solid State
Science and Technology

A Highly Sensitive Mercury Ion Sensor Based on Solid-Liquid Contact Electrification

ECS Journal of Solid State Science and Technology, 2020 **9** 115029

A Highly Sensitive Mercury Ion Sensor Based on Solid-Liquid Contact Electrification

Arnab Pal,[1] Subhodeep Chatterjee,[2] Subhajit Saha,[1] Snigdha Roy Barman,[1] Dukhyun Choi,[3,z] Sangmin Lee,[4,z] and Zong-Hong Lin[1,2,3,z]

[1]*Institute of Biomedical Engineering, National Tsing Hua University, Hsinchu 30013, Taiwan*
[2]*Department of Power Mechanical Engineering, National Tsing Hua University, Hsinchu 30013, Taiwan*
[3]*Department of Mechanical Engineering, Kyung Hee University, Yongin 17104, Republic of Korea*
[4]*School of Mechanical Engineering, Chung-Ang University, Seoul 06974, Republic of Korea*

In recent years, triboelectric nanogenerators (TENGs) are proved to be as the prime backbone for developing a self-powered sensing system. However, solid-solid contact electrification based nanogenerators suffer mostly due to inefficient contact which poses a major bottleneck for the development of long term durable and stable nanosensors. In this regard, we have reported a strategic methodology to develop a highly sensitive mercury ion sensor based on solid-liquid contact electrification, which has prime importance for the self-powered monitoring of mercury ion due to its high health risk and environmental pollution toxicity. In this work, 3-mercaptopropionic acid (MPA) capped Au nanoparticles (NPs) are employed as the solid friction layer as well as the recognition element for mercury ion detection. In addition, volatile organic solvent acetone is utilized as the contact liquid instead of water. The developed nanosensor exhibits long term stability and contact frequency independent sensing performance compared to previously reported solid-solid triboelectric nanosensors (TENS) for mercury ion detection. The large binding affinity of Hg^{2+} and the carboxylic groups results in the increase of transferred charges and enhanced surface potential. It is interesting to observe that the work function reduces after the binding of Hg^{2+} ions onto MPA molecules, which is also favorable for electron transfer during the contact electrification process. The developed nanosensor can provide a wide linear detection range from 10 nM to 1 μM as well as a low detection limit of 10 nM. As a whole, this work demonstrates a novel paradigm for designing a rapid, low-cost, and portable self-powered sensing system for real time highly selective monitoring of mercury ion from complex environmental samples.

 [DOI: 10.1149/2162-8777/abc059]

Manuscript submitted August 15, 2020; revised manuscript received October 1, 2020. Published October 27, 2020. *This paper is part of the JSS Focus Issue on Solid-State Materials and Devices for Biological and Medical Applications.*

In recent years, nanosensors have drawn major attention as an emerging technology for detecting different biological and chemical species, which facilitates the advanced development of healthcare and environmental monitoring systems.[1–3] However, an external power source such as rechargeable battery with the bulk size is essential to drive the nanosensors and thus requires an external biasing circuitry.[4–7] Meanwhile, nanogenerators have attracted considerable interest to build up self-powered systems by harvesting renewable energy from mechanical vibration,[8] sea wave,[9] wind,[10] and heat.[11] Among the different types of nanogenerators, triboelectric nanogenerators (TENGs) have drawn considerable interest as they are characterized as cost-effective, easily fabricable, and robust devices to harvest mechanical energy.[12,13] Mechanical energy can be harvested by the virtue of a periodic contact-separation process between two materials with different triboelectric polarity. When these two materials come into direct contact with each other upon applying external mechanical force, surface charge transfer occurs between them.[14–22] Consequently, the oppositely charged friction layers can create a potential drop by electrostatic induction which drives electrons in the external circuit.[23,24] As the output performance of TENG entirely depends on the magnitude, frequency and pressure of the applied mechanical force as well as on the nature of the contact materials, different physical parameters related to mechanical motion and chemical composition of the contact material surface can be analyzed using TENG.[25,26] Based on this strategy, triboelectric nanosensors (TENSs) have been developed in the recent past. Especially, TENSs can detect different chemical species such as dopamine,[27] phenol,[28] catechin,[29] thrombin,[30] and heavy metal ions[31] replacing conventional chemical sensors based on amperometry,[32] field effect,[33] potentiometry[34] or conductimetry[35] which requires external biasing circuit for sensing purpose. Recently reported most of the TENSs are driven by solid-solid contact electrification which usually suffers from several drawbacks. First, the performance of the solid-solid TENSs are highly influenced by several environmental factors such as humidity and atmospheric pressure.[36] Moreover, the continuous collision and friction between two solid surfaces with wear abrasion cause mechanical degradation of the contact materials resulting in unstable triboelectric output.[37]

According to recent research results, TENSs driven by solid-liquid contact electrification can overcome the shortcomings related to solid-solid contact electrification based TENSs. Solid-liquid TENG has been already employed to harvest ambient mechanical and electrostatic energy conveyed by different liquid[38,39] and therefore solid-liquid TENSs readily possess great potential for fabricating efficient self-powered chemical sensor.[40] Solid-liquid TENS have several advantages. As an example, shearing force with zero threshold facilitates complete contact between solid and liquid friction layers, resulting in superior triboelectric performance. Moreover, the output voltage generated by solid-liquid TENS is insensitive to ambient humidity as well as atmospheric pressure.[37] Apart from this, liquid contact layer plays an indispensable role as a lubricant which facilitates smooth movement between solid and liquid contact layer, thus improves durability as well as long-term stability of the sensor device. However, it is very difficult to entirely separate solid and liquid contact layer during contact-separation operation resulting in low electric output. Therefore, superhydrophobic solid contact surfaces have been developed in recent years by growing different nanostructure to overcome the difficulties related to surface wettability. Alternatively, high triboelectric output can also be obtained by utilizing volatile organic compounds such as ethanol and acetone as liquid contact due to their faster evaporation rate.[40]

Mercury is one of the most highly toxic metals which is potentially hazardous for the environment as well as for human health.[41] The primary health effect of mercury compounds is impaired neurological development which affects cognitive thinking, memory, attention, language, visual-spatial skills resulting in a

[z]E-mail: dchoi@khu.ac.kr; slee98@cau.ac.kr; linzh@mx.nthu.edu.tw

disease called Minamata.[42] Moreover, according to the World Health Organization (WHO), mercury can also adversely affect child's brain development and nervous system.[43] Therefore, in order to monitor mercury ion concentration in the environment as well as in biological samples, several methodologies have been employed such as atomic absorption/emission spectrometry[44] and inductively coupled plasma mass spectrometry (ICP-MS).[45] Among those reported strategies, ICP-MS method exhibits the best performance in terms of sensitivity and linear range, although it requires expensive and cumbersome instrument due to its complicated and time-consuming sample preparation method. Moreover, the methodology is not convenient for real time and on-field analysis of samples. Considering the above drawbacks, other approaches such as optical methods (systems depend on the surface plasmon resonance,[46] the surface-enhanced Raman scattering,[47] colorimetric[48] or fluorometric assays[49]) and electrochemical sensors[50] have been alternatively developed to detect the Hg^{2+} ions. Although, the above sensing strategies are convenient in terms of high sensitivity, selectivity and in-field analysis, the reported strategies are associated with complicated chemistry arising from organic probes, such as DNA, crown ethers, specific proteins, porphyrins, and polymers, which substantially restricts their utilization domain.

Here, we report self-powered mercury ion detection by portable solid-liquid TENS designed with MPA capped Au NPs as solid friction layer and acetone as contact liquid. In comparison with other NPs, Au NPs have the feature of greater long-term stability and modifiable surface chemistry.[51] Moreover, Au NPs can be synthesized with the narrow size distributions.[52] On the other hand, volatile organic solvent acetone is employed here as liquid contact due to its faster evaporation rate which ensures no residual liquid on the surface of MPA capped Au NPs upon separation of the friction layer during triboelectric operation resulting in high electric output. Detection of mercury ion is primarily controlled by the selective binding of Hg^{2+} ions with MPA ligand capped Au NPs. Therefore, surface charge density of MPA capped Au NPs surface varies according to the different concentration of Hg^{2+} ions. Under optimized circumstances, Au NPs based TENS designed in this work demonstrates a wide detection range from 10 nM to 1 μM with a low detection limit.

Experimental

Development of the solid-liquid TENS and the detection of Hg^{2+} ions.—Au NPs were deposited over copper wire using several steps through the dip coating technique. The process is schematically shown in Fig. 1. First of all, Cu wires were cleaned sequentially with acetone, ethanol, and DI water for 5 min in each solution. Then the dried Cu wires were immersed in MPA solution (10 mM) for 15 min, resulting in the binding of MPA on the Cu surface. After that, the MPA modified Cu wires were immersed in the aqueous solution of $HAuCl_4$ (2 mM) for 1 h. Then MPA was again attached over Au NPs to facilitate the subsequent detection of Hg^{2+} ions by immersing the devices in MPA solution (10 mM) for 3 h. In this step, Au NPs were capped with MPA via the Au–S bonds.[53] For the detection of mercury ion, Au NPs capped with MPA were reacted with different concentrations of $HgCl_2$ solution (0.1 nM, 1 nM, 10 nM, 100 nM, 1 μM) for 1 h.[54] Finally, the Hg^{2+} reacted samples were rinsed in DI water and dried in ambient temperature prior to various characterizations.

Material characterizations and electrical measurements.—For the insight structural and compositional studies, the fabricated samples were extensively characterized by different advanced methodologies. The surface morphology of the Au NPs on the Cu wire were characterized by using field emission scanning electron spectroscopy (FESEM, JEOL JSM-7000F). On the other hand, X-ray photoelectron spectroscopy (ESCALAB 250 XI, Thermo Scientific) equipped with an Al Kα source and hemispherical analyzer was employed for compositional analysis of the samples. All binding energies have been corrected by using C1s line at 284.6 eV, and CASA XPS software was utilized to deconvolute high resolution core level spectra. Furthermore, ultraviolet photoelectron spectroscopy (UPS) equipped with a He I light source under an ultrahigh vacuum condition was employed to measure the work function of the samples. Moreover, Kelvin probe force microscopy (KPFM) was used to probe the surface potential distribution of the samples reacted with different concentrations of Hg^{2+} ions. Finally, electrical characterizations of fabricated samples were carried out by a low-noise voltage preamplifier (Stanford Research Systems Model SR560), which was also employed to evaluate the performance of the developed solid-liquid TENS for mercury ion detection.

Electrical measurement setup for the solid-liquid TENS.—The fabricated solid-liquid TENS was based on single electrode configuration in which copper serves as the single electrode. In order to measure the electrical performance of the developed TENS, a glass container filled with acetone was placed on the stage of a dip coater system which can move in simple harmonic motion in the vertical direction to perform the submerging and emerging process with solid friction layer fabricated on the Cu wire. The calculated active contact area of the sensor was 32.2 mm^2 (wire diameter = 1 mm, length = 10 mm). The periodic contact-separation process between the solvent and active sensing area of the device generates triboelectric charges and consequent stable electric output. In order to regulate the generated electric output, a bridge rectifier circuit was employed between the TENS and SR560 electrometer. A contact frequency of 0.111 Hz has been employed for all the measurements.

The real sample detection and selectivity test of Hg^{2+} ions by the solid-liquid TENS.—In order to verify the capability of the fabricated nanosensor to detect mercury ion in real samples, different concentrations of Hg^{2+} ions (10 nM, 100 nM & 1 μM) were spiked in tap water and then the MPA capped Au NPs sensing surface of the TENS was reacted with those solutions for 1 h. After that, the samples were washed and employed for electrical characterization with acetone as the contact liquid. Furthermore, the solid friction layer was reacted with different metal ions (Na^+, K^+, Mg^{2+}, Ca^{2+}, Ba^{2+}, Cr^{3+}, Pb^{2+}, Zn^{2+} and Hg^{2+}) of same concentration (1 μM) separately in order to investigate the selectivity of the TENS towards the target ion. The voltage shift ΔV has been calculated from $| V_{metal\ ion} - V_{control} |$ where $V_{metal\ ion}$ and $V_{control}$ are the voltage responses obtained from metal ion reacted samples and control samples, respectively.

Results and Discussion

Structural and compositional analysis of TENS sensing surface.—The structural and compositional analysis of the TENS sensing area is demonstrated in Fig. 2. The successful coating of Au NPs over Cu wire was confirmed from the FESEM image as shown in Fig. 2a. The surface chemical composition of the TENS before and after Hg^{2+} ions sensing were systematically probed through high resolution XPS analysis. High resolution core-level scan of Au 4 f (Fig. 2b) reveals strong spin–orbit split components at 87.6 eV ($4f_{5/2}$) and 83.9 eV ($4\ f_{7/2}$) corresponding to metallic Au NPs. However, after the reaction with MPA and Hg^{2+} ions, the Au 4f spectrum is shifted to a higher binding energy of 0.9 eV, which indicates the formation of Au–S bonding in the samples.[55] The chemical attachment of Hg^{2+} ions through MPA is further reflected from the contribution of key functional groups of MPA in C1s and S2p core-level spectra as shown in Fig. 2c. C1s core-level spectra indicates the presence of C–C, C–S and O=C–OH bonds at 284.6 eV, 285.6 eV and 288.3 eV, respectively.[56,57] The existence of C–S bond is also confirmed from the appearance of a small peak near 164.9 eV in S2p high resolution core-level spectra. Moreover, the attachment of Hg^{2+} ions on the Au NPs is further proved from the appearance of strong Hg 4 f peaks at 104.3 eV and 100.3 eV

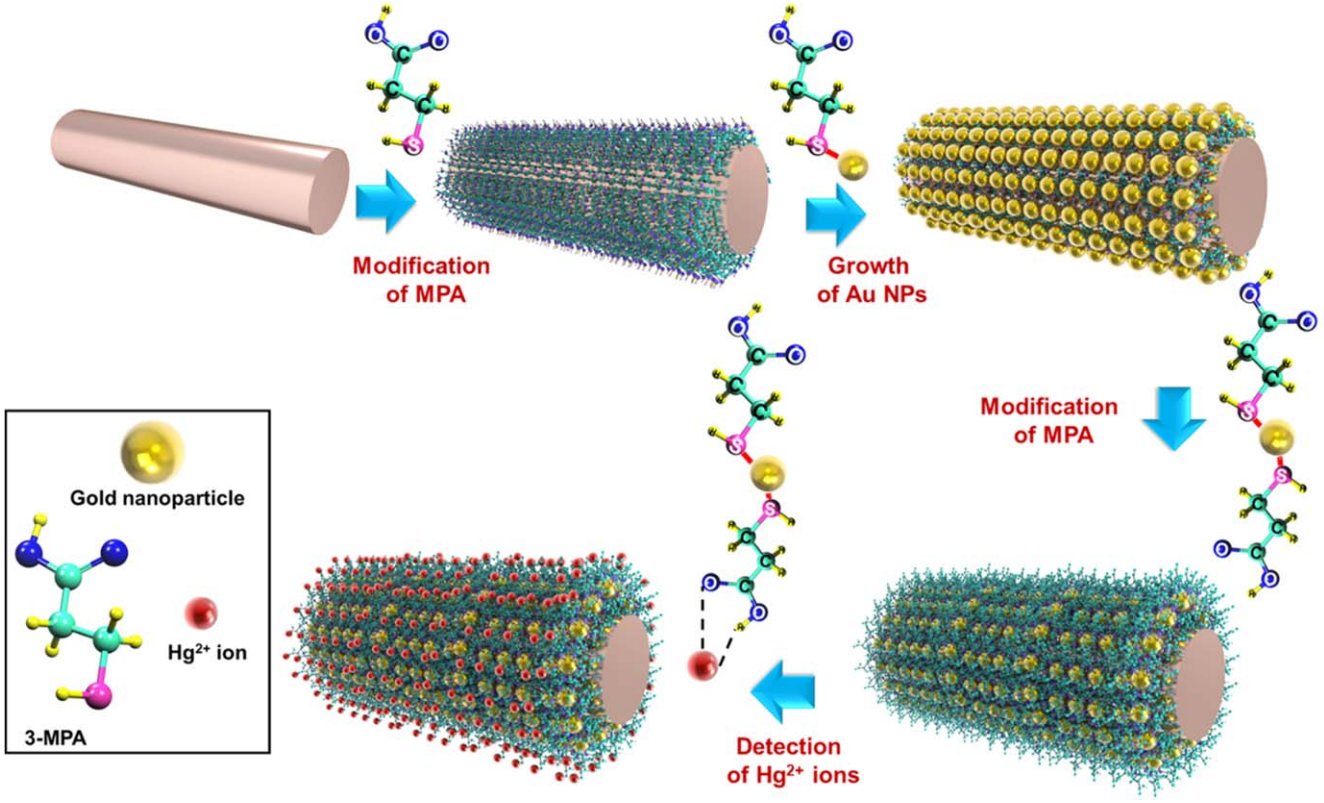

Figure 1. Schematic representation of successive steps to grow Au NPs on Cu wire and the surface of MPA modified Au NPs to detect Hg^{2+} ions. In the first step, MPA was functionalized over Cu wire surface. Then Au NPs were formed over MPA. Further, MPA was again attached over surface of Au NPs via Au-S bond. Finally, MPA capped Au NPs surface was employed to react with Hg^{2+} ions through the coordination of carboxylic groups on MPA with Hg^{2+}.

corresponding to Hg $4f_{5/2}$ and Hg $4f_{7/2}$ spin–orbit split components, respectively (Fig. 2d).[58] A careful observation towards Hg 4 f high resolution XPS peak indicates that along with metallic Hg (0), a significant amount of Hg (2+) is also present in the samples. This phenomenon strongly indicates that the Hg^{2+} ions are binding to the nanosensor surface through MPA.

The operating principle of the solid-liquid TENS.—The working principle of solid-liquid TENS is schematically illustrated in Fig. 3, where the generation of triboelectric output depends on two sequential phenomena of contact electrification and electrostatic induction.[59] Prior to the contact between the solid friction layer (Au NPs reacted with Hg^{2+} ions) and contact liquid (acetone), no charge transfer takes place in the external circuit. When Hg^{2+} ions reacted Au NPs are immersed into the liquid upon applying the mechanical force, electrons are injected to the liquid contact surface from the solid friction layer as a result of contact electrification owing to the different triboelectric polarity to gain or lose an electron.[60] Consequently, the solid friction layer becomes positively charged, and the liquid contact surface becomes negatively charged, as shown in Fig. 3a. In the next cycle, in response to another periodic mechanical force, the solid friction layer surface emerging from water leaves the negatively charged surface of the contact liquid, while positive charges still remain on the friction layer resulting in the loss of electrical equilibrium as shown in Fig. 3b. In this circumstance, to maintain the charge neutrality, electrons flow from the ground through the external circuit to the Cu electrode. The buildup potential difference reaches its maximum value upon the complete separation of the solid friction layer and contact liquid (Fig. 3c). After that, as soon as the friction layer begins to be immersed in contact liquid again, the induced charges in Cu electrode start to move back to ground (Fig. 3d) resulting in gradual decreases in the potential drop between Cu electrode and ground. Thus, a current in the reverse direction is obtained in the external circuit. The process continues until the solid friction layer makes full contact with the contact liquid, and the potential difference becomes zero as the original state is shown in Fig. 3a. Hence, a series of cyclic contact-separation processes between the friction layer and contact liquid generate periodical electrical outputs.

Investigation of the stability and sensing performance of the solid-liquid TENS.—In order to investigate the durability and stability of the developed TENS, contact-separation cycles were performed for a prolonged time of 3 h (Fig. 4b). Consequently, it is observed that there is very little deviation in the obtained output voltage even for a long-term operation indicating highly stable triboelectric performance of the solid-liquid TENS due to the lubricating property of the contact liquid, which facilitates smooth movement of the solid friction layer into liquid environment. The FESEM image as shown in Fig. 4a further confirms the structural integrity of surface morphology of the sensing area even after a prolonged operation time, which facilitates long term stable triboelectric output. Moreover, the triboelectric performance of the TENS was also investigated in terms of different contact frequencies ranging from 0.072 Hz to 0.111 Hz as shown in Fig. 4c. The obtained electrical output suggests that the output response is independent of contact frequency as there is very little influence of rapid fluctuation of solid-liquid interfacial surface charge density on the triboelectric performance of TENS due to fast evaporation rate of acetone from the solid friction layer. All the obtained experimental results strongly indicate the long-term stability and durability of solid-liquid triboelectric system in comparison with solid-solid triboelectric system as reported previously. On the other hand, Fig. 5a exhibits the sensing performance of the TENS for different concentration of mercury ion. The output voltage is enhanced from 213 mV to 258 mV with the increasing concentrations of mercury ion ranging from 0.1 nM to 1 μM. The reason behind the higher shift of the output voltage can be explained in terms of surface charge

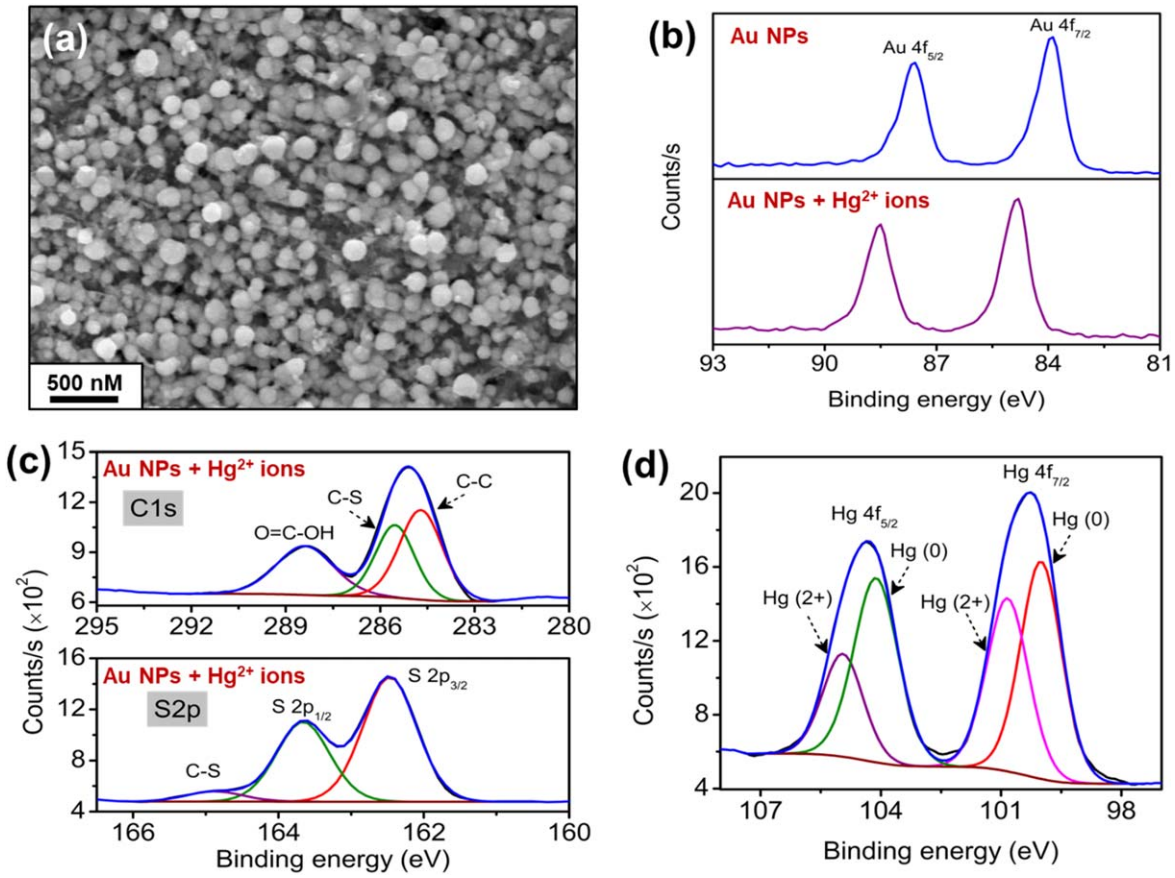

Figure 2. (a) FESEM image of synthesized Au NPs on Cu wire. (b) High-resolution XPS for Au 4f levels revealing the higher binding energy shift after the binding with Hg^{2+} ions. (c)–(d) High-resolution XPS for C 1s, S 2p and Hg 4f levels revealing the binding of Hg^{2+} ions onto Au NPs surface via MPA.

density and triboelectric polarity. With the increasing concentrations of Hg^{2+} ions incorporated on the surface of MPA capped Au NPs, surface charge density of the solid friction layer is enhanced which results from the higher difference in triboelectric polarity between the contact liquid and the solid friction layer. Furthermore, Fig. 5b demonstrates the calibration curve for the sensing performance obtained for different concentrations of Hg^{2+} ions. The output result indicates lower detection limit of 10 nM and wide linear range from 10 nM to 1 μM, which satisfies the concentration limits of Hg^{2+} ions in the drinking water recommended by the World Health Organization (30 nM) and the U.S. Environmental Protection Agency (10 nM).[61] Thus, the calibration curve indicates the reliability and repeatability of the developed TENS which has great potential to monitor the concentration of Hg^{2+} ions in real samples. The long-range linearity and ultralow detection limit have been achieved by the virtue of the utilization of acetone as contact liquid which is one of the most crucial parameters for the sensing performance. Moreover, high selectivity of Hg^{2+} ions towards MPA capped Au NPs also play an indispensable role to achieve higher sensitivity for mercury ion detection.

Sensing mechanism for mercury ion detection.—Hg^{2+} ions attached with MPA capped Au NPs demonstrate enhanced output performance as a result of the increased interfacial charge transfer process between the contact liquid and solid friction layer. Hg^{2+} and carboxylic groups of MPA has a strong binding affinity towards each other.[62,63] In order to investigate the interfacial surface charge transfer phenomena, the surface potential of the solid friction layer was characterized by Kelvin probe force microscopy(KPFM) as shown in Fig. 6a. The surface potential distribution measured by KPFM clearly indicates the consistent enhancement of surface potential ranging from −165.95 mV to −39.74 mV with increasing concentrations of Hg^{2+} ions from 0 to 1 μM. The obtained KPFM results suggest that potential difference between the Cu electrode and the contact liquid increases upon the binding with Hg^{2+} ions onto the solid friction layer, which drives more electrons flowing between ground and the Cu electrode. The result also indicates that the positional difference between the contact liquid and the solid friction layer is enhanced in triboelectric series as Hg^{2+} ions reacted Au NPs is placed into more positive side due to the higher surface potential shift with respect to the pristine solid friction layer. Moreover, work function change of the solid friction layer was also investigated by ultra-violet photoelectron spectroscopy (UPS) (Fig. 6b) in order to obtain a further explanation of higher surface potential shift as indicated by KPFM. Applying the equation $\Phi = 21.22 - (E_{Fermi} - E_{cut\text{-}off})$,[64] the work function (Φ) was calculated for the Au NPs before and after incorporation of Hg^{2+} ions (Fig. 6c). According to the result, the reduction in work function after incorporation of mercury ion over solid friction layer promotes easier electron transfer by lowering the surface potential barrier.

Detection of mercury ion in tap water and selectivity test.—The highly selective nature of the as-designed TENS indicates the feasibility of employing the nanosensor for in-field and real-time detection of Hg^{2+} ions. Subsequently, the real-time sensing capability of the as developed nanosensing platform was evaluated by quantifying the concentration of Hg^{2+} ions in tap water. Prior to the sensing measurement, the water samples were centrifuged and filtered in order to separate out the impurities. Then, the tap water sample was spiked with the different concentrations of Hg^{2+} ions (10 nM, 100 nM and 1 μM). Figure 7a exhibits the electric output of the TENS for different concentrations of Hg^{2+} ions spiked in tap water. From the result, it is clearly visible that the output voltage of the TENS is reduced as compared to TENS device reacted with

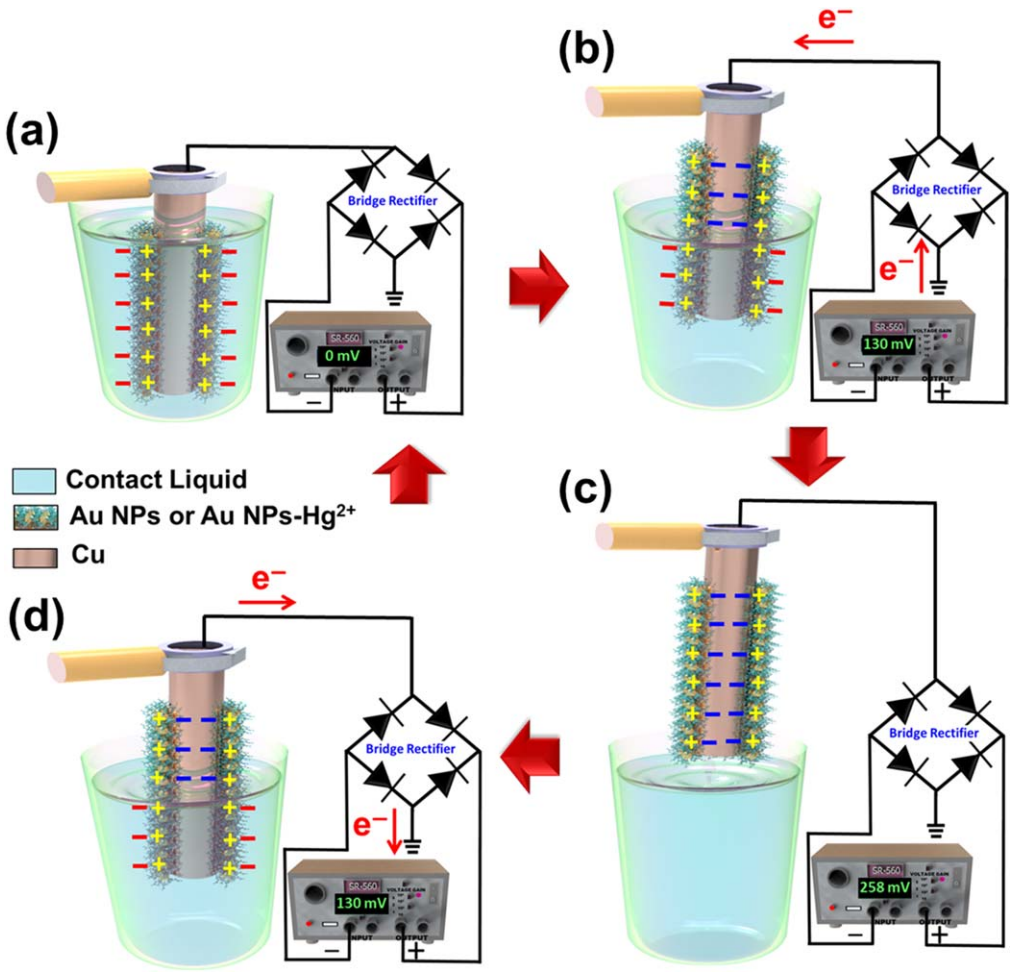

Figure 3. The working mechanism illustration of the Au NPs based solid-liquid TENS. (a) When the solid friction layer (Au NPs or Au NPs-Hg^{2+}) is immersed in contact liquid, the contact electrification results in solid surface to bring positive charges and liquid surface to bring negative charges. (b)–(c) Once the separation process proceeds, generated potential induces electron flow from the ground to the Cu wire until it gains the equilibrium. The induced negative charges on the Cu electrode are shown in blue color. (d) Further the solid friction layer starts to be immersed in the liquid again resulting in the reduction of potential difference which drives electron flow back from the Cu wire to the ground until the potential difference returns to zero as the original status (a).

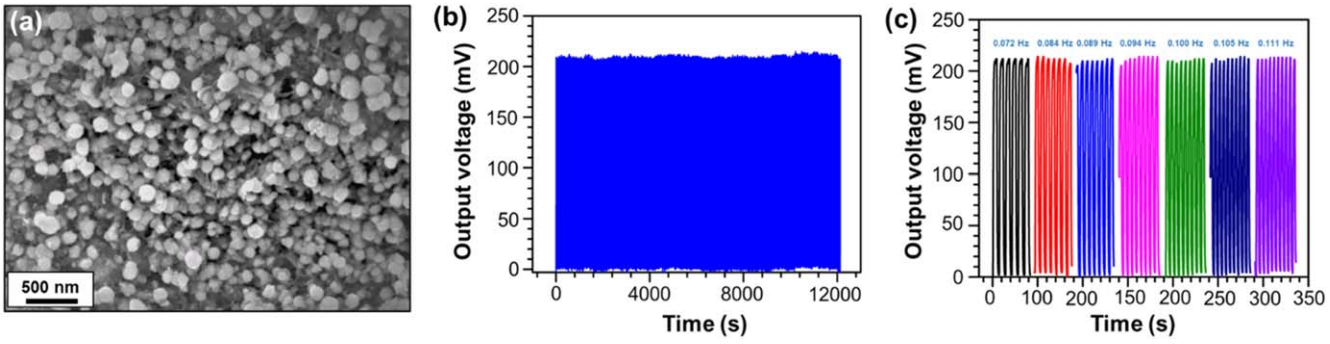

Figure 4. (a) FESEM image of 3-MPA modified AuNPs surface after 3 h of contact-separation operation. (b) Investigation of the durability and stability of solid-liquid TENS for a time span of more than 3 h. (c) Output voltage cycles of solid-liquid TENS for different contact frequencies.

standard Hg^{2+} ion solutions prepared in deionized water. The reduction in the output voltage can be attributed to the fact that the real water samples are comprised of different metal ions which possess a high probability of getting absorbed onto the solid friction layer surfaces during the contact-electrification process. It facilitates an incomplete screening of triboelectric charges on the nanosensor's surface thereby resulting in reduced output voltage.[31] Despite this factor, the obtained electrical output (Fig. 7a) clearly indicates that the TENS is capable of detecting even lower concentration of Hg^{2+} ions (10 nM) dissolved in real samples. However, the real sample contains numerous metal ions which may interfere with the sensing performance of our fabricated device. Therefore, in order to investigate the selectivity of our TENS towards mercury ions, the sensor surface was also reacted with solution containing other interfering metal ions (Na^{+}, K^{+}, Mg^{2+}, Ca^{2+}, Ba^{2+}, Cr^{3+}, $Pb^{2+}$and Zn^{2+}) of the same concentration (1 μM) as well as Hg^{2+} ions and the sensing performance of the TENS was investigated (Fig. 7b). The results shown in Fig. 7b exhibit the triboelectric

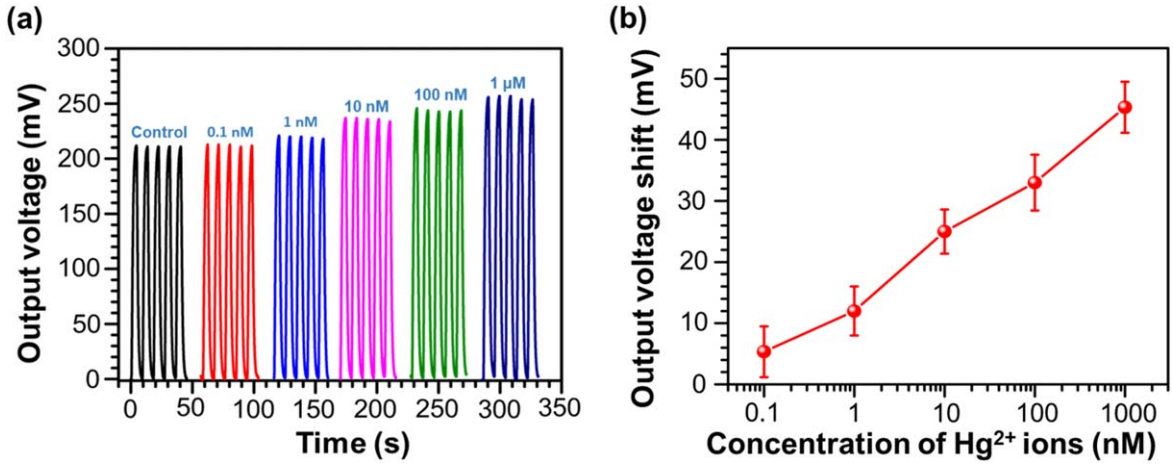

Figure 5. (a) The output voltage and (b) calibration curve of the solid-liquid TENS when detecting different concentrations of Hg^{2+} ions. Acetone is selected as the contact liquid.

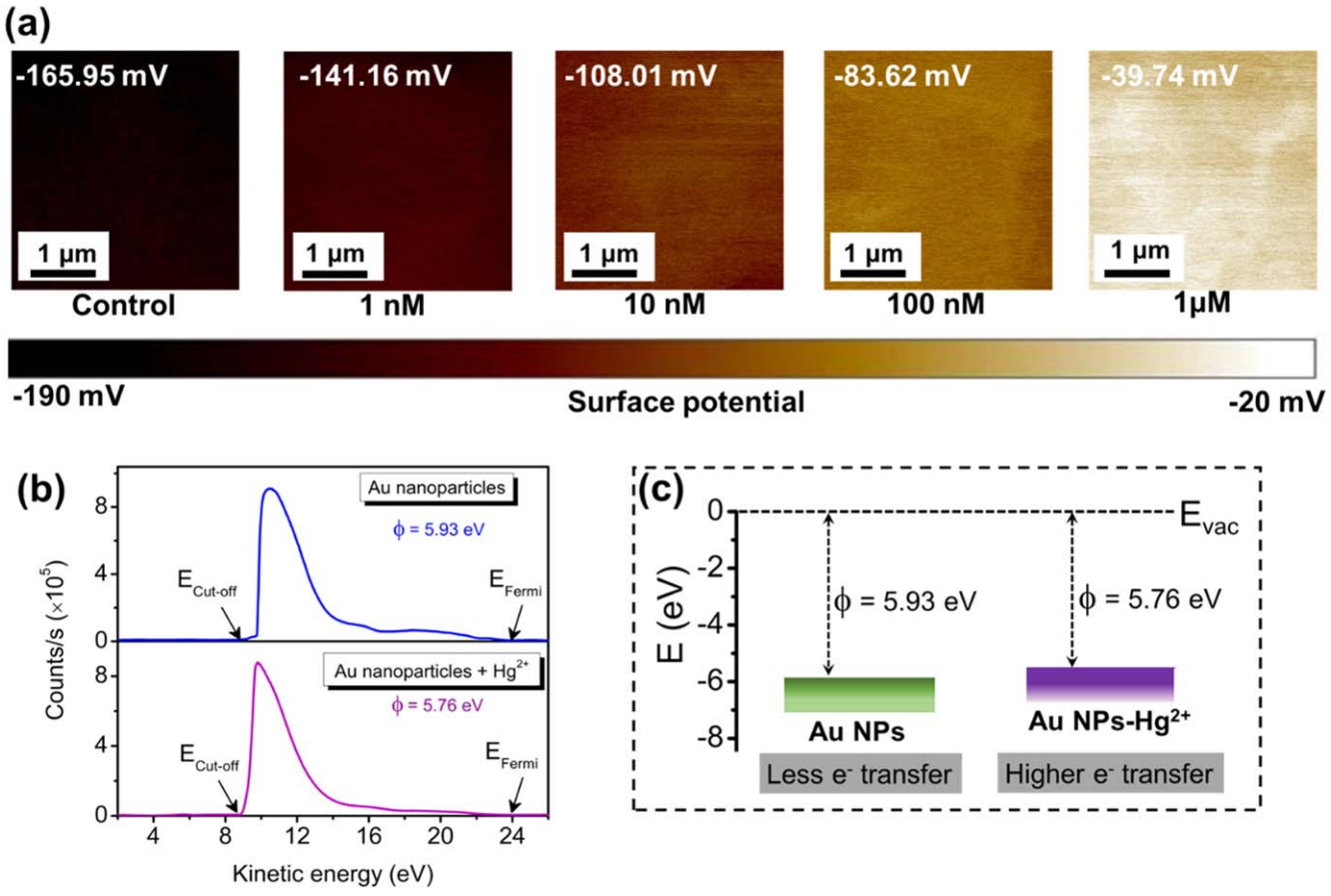

Figure 6. (a) KPFM data of the Au NPs surface when binding with different concentrations of Hg^{2+} ions. (b) UPS spectra of the Au NPs before and after the binding of Hg^{2+} ions. Inset arrows indicate the positions of the Fermi level (E_{Fermi}) and secondary electron cut-off energy ($E_{cut\text{-}off}$). (c) Schematic representation of the work function reduction of the Au NPs surface upon the binding with Hg^{2+} ions.

output voltage shift for the different metal ions. It is observed that the response voltage obtained from the TENS reacted with Hg^{2+} ions are 3 times and 5 times higher than that of Pb^{2+} ions and the rest of the metal ions respectively. The primary reason behind this high selectivity of the TENS can be interpreted by the inherent ability of MPA ligand to selectively bind Hg^{2+} ions by the formation of coordination bond with the carboxyl group of MPA through chelation. In contrast, the poor interaction between other metal ions with the sensing surface results in very low output response. The result indicates high selectivity and sensitivity of our TENS towards Hg^{2+} ion detection. Moreover, all the obtained results strongly suggest the practical applicability of the solid-liquid TENS for real time and on-field analysis.

Conclusions

In summary, solid-liquid TENS was employed for the first time for self-powered detection of Hg^{2+} ions by utilizing MPA capped Au NPs as the solid friction layer and volatile solvent acetone as the

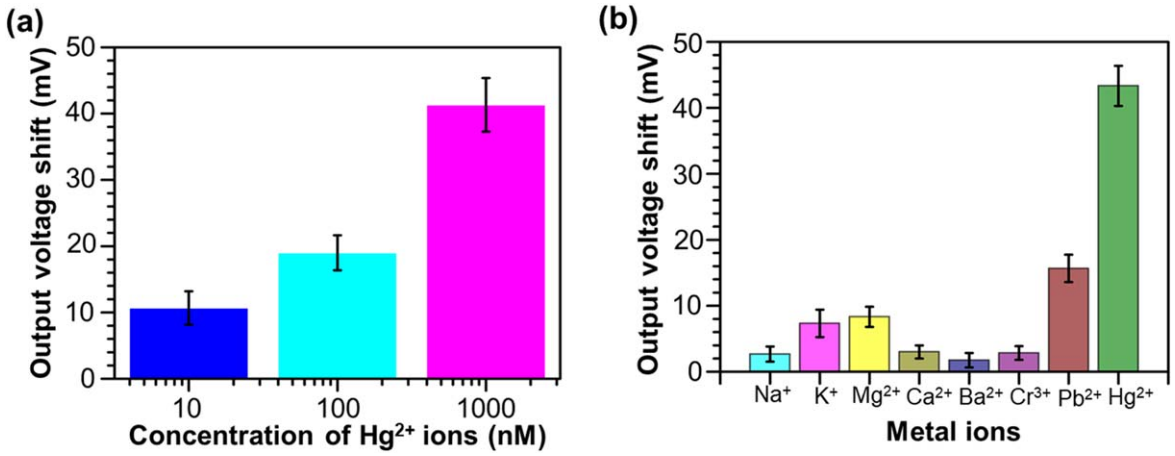

Figure 7. (a) Output voltage response of the triboelectric nanosensor upon detection of different concentrations of spiked Hg^{2+} ions in tap water. (b) The selectivity performance of the TENS as a self-powered Hg^{2+} ion sensor at a particular concentration of 1 μM of different metal ions.

contact liquid. The strong binding affinity of Hg^{2+} ions towards MPA ligand reduces the work-function of the solid friction layer which further facilitates enhanced interfacial charge transfer between the solid friction layer and the contact liquid. On the other hand, volatile organic solvent acetone as contact liquid contributes to generate higher triboelectric output eliminating the necessity of hydrophobic solid friction layer in case of solid-liquid contact electrification. Moreover, in contrast with solid-solid TENS, our solid-liquid TENS also provides long term stability and contact frequency independent triboelectric output. Furthermore, the self-powered solid-liquid TENS provides a wide detection range from 10 nM to 1 μM and a low detection limit of 10 nM. In addition, the detection of mercury ions in tap water allows to develop stand-alone, cost-effective, simple and user-friendly nanosensor for on-field environmental monitoring purposes. It is believed that the designed prototype self-powered nanosensor opens a new window towards the future development of triboelectric effect based nanosensor for detection of other metal ions as well as biomolecules like DNA, proteins and pathogens.

Acknowledgments

The authors would like to thank the Ministry of Science and Technology (MOST 109-2636-E-007-013) and the National Tsing Hua University in Taiwan for financially supporting this research. This research was also supported by the Chung-Ang University Research Grant in 2020.

ORCID

Zong-Hong Lin https://orcid.org/0000-0002-1793-7858

References

1. L. Jin, J. Chen, B. Zhang, W. Deng, L. Zhang, H. Zhang, X. Huang, M. Zhu, W. Yang, and Z. L. Wang, *ACS Nano*, **10**, 7874 (2016).
2. Y. K. Fuh, P. C. Chen, Z. M. Huang, and H. C. Ho, *Nano Energy*, **11**, 671 (2015).
3. L. Dhakar, P. Pitchappa, F. E. H. Tay, and C. Lee, *Nano Energy*, **19**, 532 (2016).
4. S.-M. Xu, X. Liang, X.-Y. Wu, S.-L. Zhao, J. Chen, K.-X. Wang, and J.-S. Chen, *Nat. Commun.*, **10**, 5810 (2019).
5. G. Zan, T. Wu, P. Hu, Y. Zhou, S. Zhao, S. Xu, J. Chen, Y. Cui, and Q. Wu, *Energy Storage Mater.*, **28**, 82 (2020).
6. W. Liu, J. Chen, Z. Chen, K. Liu, G. Zhou, Y. Sun, M.-S. Song, Z. Bao, and Y. Cui, *Adv. Energy Mater.*, **7**, 1701076 (2017).
7. H. Yin, K. S. Hui, X. Zhao, S. Mei, X. Lv, K. N. Hui, and J. Chen, *ACS Appl. Energy Mater.*, **3**, 6897 (2020).
8. Y. Qin, X. Wang, and Z. L. Wang, *Nature*, **451**, 809 (2008).
9. D. Y. Kima, H. S. Kima, D. S. Konga, M. Choib, H. B. Kima, J.-H. Leec, G. Murillod, M. Leeb, S. S. Kimc, and J. H. Junga, *Nano Energy*, **45**, 247 (2018).
10. B. Dudema, N. D. Huynhb, W. Kimb, D. H. Kima, H. J. Hwangb, D. Choib, and J. S. Yua, *Nano Energy*, **42**, 269 (2017).
11. Y. Yang, W. Guo, K. C. Pradel, G. Zhu, Y. Zhou, Y. Zhang, Y. Hu, L. Lin, and Z. L. Wang, *Nano Lett.*, **12**, 2833 (2012).
12. F. R. Fan, Z. Q. Tian, and Z. L. Wang, *Nano Energy*, **1**, 328 (2012).
13. F. R. Fan, L. Lin, G. Zhu, W. Wu, R. Zhang, and Z. L. Wang, *Nano Lett.*, **12**, 3109 (2012).
14. J. Chen, Y. Huang, N. Zhang, H. Zou, R. Liu, C. Tao, X. Fan, and Z. L. Wang, *Nat. Energy*, **1**, 16138 (2016).
15. G. Chen, Y. Li, M. Bick, and J. Chen, *Chem. Rev.*, **120**, 3668 (2020).
16. Y. Zhou, W. Deng, J. Xu, and J. Chen, *Cell Rep. Phys. Sci.*, **1**, 100142 (2020).
17. Y. Zou, V. Raveendran, and J. Chen, *Nano Energy*, **77**, 105303 (2020).
18. Y. Su et al., *Nano Energy*, **74**, 104941 (2020).
19. Y. Su et al., *ACS Nano*, **14**, 6067 (2020).
20. K. Meng et al., *Matter*, **2**, 896 (2020).
21. Z. Zhou et al., *Biosens. Bioelectron.*, **155**, 112064 (2020).
22. Z. Zhou et al., *Nat Electron*, **3**, 571 (2020).
23. G. Zhu, C. Pan, W. Guo, C.-Y. Chen, Y. Zhou, Z. Yu, and Z. L. Wang, *Nano Lett.*, **12**, 4960 (2012).
24. G. Zhu, Z.-H. Lin, Q. Jing, P. Bai, C. Pan, Y. Yang, Y. Zhou, and Z. L. Wang, *Nano Lett.*, **13**, 847 (2013).
25. S. Wang, L. Lin, Y. Xie, Q. Jing, S. Niu, and Z. L. Wang, *Nano Lett.*, **13**, 2226 (2013).
26. G. Cheng, Z. H. Lin, L. Lin, Z. L. Du, and Z. L. Wang, *ACS Nano*, **7**, 7383 (2013).
27. X. Zhang, Y. Zheng, D. Wang, Z. U. Rahman, and F. Zhou, *Nano Energy*, **30**, 321 (2016).
28. Z. Li, J. Chen, J. Yang, Y. Su, X. Fan, Y. Wu, C. Y., and Z. L. Wang, *Energy Environ. Sci.*, **8**, 887 (2015).
29. Z.-H. Lin, Y. Xie, Y. Yang, S. Wang, G. Zhu, and Z. L. Wang, *ACS Nano*, **7**, 4554 (2013).
30. Y. K. Jung, K. N. Kim, J. M. Baik, and B. S. Kim, *Nano Energy*, **30**, 77 (2016).
31. Z. Li, J. Chen, H. Guo, X. Fan, Z. Wen, M.-H. Yeh, C. Yu, X. Cao, and Z. L. Wang, *Adv. Mater.*, **28**, 2983 (2016).
32. K. Y. Inoue et al., *Lab Chip*, **12**, 3481 (2012).
33. J. M. Rothberg et al., *Nature*, **475**, 348 (2011).
34. H. Suzuki, H. Shiroishi, S. Sasaki, and I. Karube, *Anal. Chem.*, **71**, 5069 (1999).
35. E. S. Forzani, X. Li, and N. Tao, *Anal. Chem.*, **79**, 5217 (2007).
36. V. Nguyen and R. Yang, *Nano Energy*, **2**, 604 (2013).
37. X. Zhang, Y. Zheng, D. Wang, and F. Zhou, *Nano Energy*, **40**, 95 (2017).
38. D. Choi, S. Lee, S. M. Park, H. Cho, W. Hwang, and D. S. Kim, *Nano Res.*, **8**, 2481 (2015).
39. Z.-H. Lin, G. Cheng, S. Lee, K. C. Pradel, and Z. L. Wang, *Adv. Mater.*, **26**, 4690 (2014).
40. S. Chatterjee, S. Saha, S. R. Barman, I. Khan, Y.-P. Pao, S. Lee, D. Choi, and Z.-H. Lin, *Nano Energy*, **77**, 105093 (2020).
41. M. Aschner and J. L. Aschner, *Neurosci. Biobehav. Rev.*, **14**, 169 (1990).
42. A. K. James et al., *Environ. Sci. Technol.*, **54**, 2726 (2020).
43. T. W. Clarkson, L. Magos, and G. J. Myers, *N. Engl. J. Med.*, **349**, 1731 (2003).
44. C. P. Hanna, J. F. Tyson, and S. McIntosh, *Anal. Chem.*, **65**, 653 (1993).
45. M. Leermakers, W. Baeyens, P. Quevauviller, and M. Horvat, *TrAC - Trends Anal. Chem.*, **24**, 383 (2005).
46. C. sar Díez-Gil, R. Martínez, I. Ratera, T. Hirsh, A. Espinosa, A. Tárraga, P. Molina, O. S. Wolfbeisd, and J. Veciana, *Chem. Commun.*, **47**, 1842 (2011).
47. T. Senapati, D. Senapati, A. K. Singh, Z. Fan, R. Kanchanapally, and P. C. Ray, *Chem. Commun.*, **47**, 10326 (2011).
48. J. S. Lee, M. S. Han, and C. A. Mirkin, *Angew. Chemie—Int. Ed.*, **46**, 4093 (2007).
49. J. V. Ros-Lis, M. D. Marcos, R. Mártinez-Máñez, K. Rurack, and J. Soto, *Angew. Chemie—Int. Ed.*, **44**, 4405 (2005).
50. H. Park, S. J. Hwang, and K. Kim, *Electrochem. Commun.*, **24**, 100 (2012).
51. G. K. Darbha, A. K. Singh, U. S. Rai, E. Yu, H. Yu, and P. C. Ray, *J. Am. Chem. Soc.*, **130**, 8038 (2008).
52. C. Fang, Y. Fan, J. M. Kong, Z. Q. Gao, and N. Balasubramanian, *Appl. Phys. Lett.*, **92**, 2 (2008) .
53. C. C. Huang and H. T. Chang, *Chem. Commun.*, **12**, 1215 (2007).

54. D. E. Li and C. H. Lin, *RSC Adv.*, **8**, 16139 (2018).
55. C. Battocchio, F. Porcaro, S. Mukherjee, E. Magnano, S. Nappini, l. Fratoddi, M. Quintiliani, M. V. Russo, and G. Polzonetti, *J. Phys. Chem. C*, **118**, 8159 (2014).
56. Y. Wu, Y. Lin, and J. Xu, *Photochem. Photobiol. Sci.*, **18**, 1081 (2019).
57. Z. Wang, Y. Dong, H. Li, Z. Zhao, H. B. Wu, C. Hao, S. Liu, J. Qiu, and X. W. Lou, *Nat. Commun.*, **5** (2014).
58. S. Yang, Y. Guo, N. Yan, Z. Qu, J. Xie, C. Yang, and J. Jia, *J. Hazard. Mater.*, **186**, 508 (2011).
59. Z.-H. Lin, G. Cheng, L. Lin, S. Lee, and Z. L. Wang, *Angew. Chemie - Int. Ed.*, **52**, 12545 (2013).
60. H. Zou et al., *Nat. Commun.*, **10**, 1 (2019).
61. J. Liu and Y. Lu, *Angew. Chemie*, **119**, 7731 (2007).
62. E. Ertem, M. Diez-Castellnou, Q. K. Ong, and F. Stellacci, *Chem. Rec.*, **18**, 819 (2018).
63. I. J. Gomez, B. Arnaiz, M. Cacioppo, F. Arcudi, and M. Prato, *J. Mater. Chem. B*, **6** (2018).
64. Y. E. Ha, G. E. Lim, M. Y. Jo, J. Park, Y.-C. Kang, S.-J. Moonc, and J. H. Kim, *J. Mater. Chem. C*, **2**, 3820 (2014).